

โครงสร้างระดับนาโนเมตรของเงินแบบลำดับชั้นจากซิลเวอร์แอซีเทตที่ถูกรีดิวซ์ด้วยไฮโดรเจนเปอร์ออกไซด์



นายปรินทร แจ้งทวี

จุฬาลงกรณ์มหาวิทยาลัย

CHULALONGKORN UNIVERSITY

บทคัดย่อและแฟ้มข้อมูลฉบับเต็มของวิทยานิพนธ์ตั้งแต่ปีการศึกษา 2554 ที่ให้บริการในคลังปัญญาจุฬาฯ (CUIR) เป็นแฟ้มข้อมูลของนิสิตเจ้าของวิทยานิพนธ์ ที่ส่งผ่านทางบัณฑิตวิทยาลัย

The abstract and full text of theses from the academic year 2011 in Chulalongkorn University Intellectual Repository (CUIR) are the thesis authors' files submitted through the University Graduate School.

วิทยานิพนธ์นี้เป็นส่วนหนึ่งของการศึกษาตามหลักสูตรปริญญาวิทยาศาสตรมหาบัณฑิต

สาขาวิชาเคมี ภาควิชาเคมี

คณะวิทยาศาสตร์ จุฬาลงกรณ์มหาวิทยาลัย

ปีการศึกษา 2557

ลิขสิทธิ์ของจุฬาลงกรณ์มหาวิทยาลัย

HIERARCHICAL SILVER NANOSTRUCTURE FROM HYDROGEN PEROXIDE-
REDUCED SILVER ACETATE

Mr. Parinton Jangtawee



A Thesis Submitted in Partial Fulfillment of the Requirements
for the Degree of Master of Science Program in Chemistry
Department of Chemistry
Faculty of Science
Chulalongkorn University
Academic Year 2014
Copyright of Chulalongkorn University

Thesis Title	HIERARCHICAL SILVER NANOSTRUCTURE FROM HYDROGEN PEROXIDE-REDUCED SILVER ACETATE
By	Mr. Parinton Jangtawee
Field of Study	Chemistry
Thesis Advisor	Associate Professor Sanong Ekgasit
Thesis Co-Advisor	Associate Professor Chuchaat Thammacharoen

Accepted by the Faculty of Science, Chulalongkorn University in Partial Fulfillment of the Requirements for the Master's Degree

.....Dean of the Faculty of Science
(Professor Supot Hannongbua)

THESIS COMMITTEE

.....Chairman
(Associate Professor Vudhichai Parasuk)

.....Thesis Advisor
(Associate Professor Sanong Ekgasit)

.....Thesis Co-Advisor
(Associate Professor Chuchaat Thammacharoen)

.....Examiner
(Professor Thawatchai Tuntulani)

.....External Examiner
(Associate Professor Chinapong Kritayakornupong)

ปริญญ์ แจ่มทวิ : โครงสร้างระดับนาโนเมตรของเงินแบบลำดับชั้นจากซิลเวอร์แอซีเทตที่
 ถูกรีดิวซ์ด้วยไฮโดรเจนเปอร์ออกไซด์ (HIERARCHICAL SILVER NANOSTRUCTURE
 FROM HYDROGEN PEROXIDE-REDUCED SILVER ACETATE) อ.ที่ปรึกษาวิทยานิพนธ์
 หลัก: รศ. ดร.สนอง เอกสิทธิ์, อ.ที่ปรึกษาวิทยานิพนธ์ร่วม: รศ. ชูชาติ ธรรมเจริญ, 50
 หน้า.

โลหะเงินในระดับไมโครเมตรถูกสังเคราะห์ขึ้นจากปฏิกิริยาเคมีภายใต้อุณหภูมิห้องและ
 ความดันบรรยากาศภายในระยะเวลา 2 นาที ซึ่งเป็นปฏิกิริยาระหว่างซิลเวอร์แอซีเทตและไฮโดรเจน
 เปอร์ออกไซด์โดยปราศจากสารลดแรงตึงผิวหรือสารเกาะพื้นผิวอื่น โลหะเงินในระดับไมโครเมตร
 ได้รับการพิสูจน์เอกลักษณ์ด้วยวิธีการทางสเปกโทรสโกปีต่างๆ รวมถึงการพิสูจน์รูปร่างโครงสร้างด้วย
 รังสีเอ็กซ์แสดงโครงสร้างแบบเดนดริติก การควบคุมอัตราเร็วของปฏิกิริยาสามารถควบคุมรูปร่างของ
 โครงสร้างโลหะเงินในระดับไมโครเมตรได้ อีกทั้งแอซีเทตไอออนซึ่งเป็นไอออนที่หลงเหลือในปฏิกิริยา
 ยังเกาะกับผิวของโลหะเงินเกิดความไม่ชอบน้ำขึ้นบนพื้นผิว ทำให้ตัวทำละลายอินทรีย์สามารถเกิด
 อันตรกิริยากับโลหะเงินได้ โลหะเงินในระดับไมโครเมตรหลายๆแบบซึ่งได้จากการสังเคราะห์ด้วย
 สภาวะที่ต่างกันได้ถูกทดสอบความสามารถในการเพิ่มสัญญาณรามานโดยใช้สารละลายโรห์ตามีน
 ซิกซ์จีเป็นสารมาตรฐาน ซึ่งความสามารถในการเพิ่มสัญญาณขึ้นอยู่กับความขรุขระของพื้นผิวที่
 นำไปสู่ช่องว่างในระดับนาโนเมตรซึ่งสร้างคลื่นแม่เหล็กไฟฟ้าให้กับโมเลกุลที่อยู่ระหว่างช่องว่างนั้น
 โลหะเงินในระดับไมโครเมตรที่มีความสามารถในการเพิ่มสัญญาณดีที่สุดได้ถูกนำไปทดสอบสาร
 ปนเปื้อนที่ออกมาจากพลาสติกห่ออาหาร

จุฬาลงกรณ์มหาวิทยาลัย
 CHULALONGKORN UNIVERSITY

ภาควิชา	เคมี	ลายมือชื่อนิสิต
สาขาวิชา	เคมี	ลายมือชื่อ อ.ที่ปรึกษาหลัก
ปีการศึกษา	2557	ลายมือชื่อ อ.ที่ปรึกษาร่วม

5572037023 : MAJOR CHEMISTRY

KEYWORDS: AG NANOSTRUCTURE / DENDRITE / ACETATE / SERS

PARINTON JANGTAWEE: HIERARCHICAL SILVER NANOSTRUCTURE FROM HYDROGEN PEROXIDE-REDUCED SILVER ACETATE. ADVISOR: ASSOC. PROF. SANONG EKGASIT, CO-ADVISOR: ASSOC. PROF. CHUCHAAT THAMMACHAROEN, 50 pp.

Ag microstructures were synthesized with a reaction between silver acetate (CH_3COOAg) and hydrogen peroxide (H_2O_2) without surfactant or capping agent under ambient condition in 2 min. They were characterized with spectroscopy techniques. Ag microstructures showed dendritic pattern on their surface with single crystal XRD pattern. Rate of the reaction plays an important role on structural control. Acetate ion spontaneously binds with Ag surface and organic solvents with the other end. Ag microstructures were also controlled by changing the surface property. Different Ag microstructures synthesized from different conditions were tested on SERS with R6G as the probe molecule. Roughness on the Ag surface represents dendritic pattern which provides nanogaps to enhance the Raman signal. The migration of plasticizers from food wraps was detected by SERS technique using Ag microstructures as the substrate. Moreover, growth evolution of Ag microstructures was also discussed.

จุฬาลงกรณ์มหาวิทยาลัย
CHULALONGKORN UNIVERSITY

Department: Chemistry

Field of Study: Chemistry

Academic Year: 2014

Student's Signature

Advisor's Signature

Co-Advisor's Signature

ACKNOWLEDGEMENTS

I would like to express my sincere gratitude to my thesis advisor, Associate Professor Dr. Sanong Ekgasit and my thesis co-advisor Associate Professor Chuchaat Thammacharoen for giving me an invaluable opportunity to be a good researcher. I am also thankful for all thesis committees who corrected this thesis.

Warmest thanks to my friends, my colleagues and organization: Sensor Research Unit, Department of Chemistry, Faculty of Science, Chulalongkorn University, and all relationships I have got during my two and a half years in Bangkok.

Whatever shortcomings in the thesis remain, they are the sole responsibility of the author.

Finally, I am profoundly grateful to my parents and endearing family for all their loves, understanding, support, and encouragement during the whole period of study.

CONTENTS

	Page
THAI ABSTRACT	iv
ENGLISH ABSTRACT	v
ACKNOWLEDGEMENTS	vi
CONTENTS	vii
REFERENCES	48
VITA.....	50



List of figures

Figure		Page
2.1	Energy-level diagram showing the states involved in Raman signal.	5
2.2	Illustration of the excitation of the LSPRs of a spherical nanoparticle by incident electromagnetic radiation.	6
2.3	Theoretical simulations of the electromagnetic field enhancement around silver nanoparticles of (A) a triangular nanoparticle (700 nm), (B) a dimer of spherical nanoparticles (520 nm), and (C) an ellipsoidal nanoparticle (695 nm).	7
4.1	Optical and spectroscopic information of synthesized white silver acetate powder: (A) photographic image, (B) optical microscope image (100X magnification), (C) SEM image and (D) Raman spectrum.	13
4.2	Ag microstructures prepared by a wet chemical reaction between silver acetate and hydrogen peroxide without surfactant or capping agent: (A) photographic image of the microstructures suspended in the reaction media, (B) optical microscope image (400X), and (C) SEM image.	14
4.3	SEM images of Ag microstructures prepared by a wet chemical reaction between silver acetate and hydrogen peroxide without surfactant or capping agent: (A) as-synthesized and (B) 24 h incubation in the reaction media. The scale bars indicate 5 μm .	15
4.4	Elemental analysis of Ag microstructures: (A) SEM image, (B) EDS silver map, (C) EDS oxygen map, (D) EDS carbon map, (E) EDS spectrum, and (F) XRD pattern.	16

- 4.5 SEM images of Ag microstructures synthesized by reducing silver acetate with 31 mM hydrogen peroxide. The concentrations of silver acetate are: (A) 200 mM, (B) 267 mM, (C) 334 mM, (D) 400 mM, (E) 467 mM, and (F) 534 mM. The scale bars indicate 5 μm . 17
- 4.6 SEM images of Ag microstructures synthesized by reducing silver acetate with various concentrations of hydrogen peroxide: (A) 3 mM, (B) 15 mM, (C) 31 mM, (D) 154 mM, (E) 309 mM, and (F) 617 mM. The scale bars indicate 5 μm . 19
- 4.7 SEM images of Ag microstructures synthesized by reducing 0.667M silver acetate with 31 mM hydrogen peroxide. The concentrations of added sodium acetate are: (A) 0 M, (B) 0.667 M, (C) 2.668 M, (D) 4.002 M, (E) 5.336 M, and (F) 6.67 M. The scale bars indicate 5 μm . 20
- 4.8 SEM images of Ag microstructures synthesized by reducing 0.667 M silver acetate with 31 mM hydrogen peroxide. The pH of hydrogen peroxide are: (A) 5, (B) 6, (C) 7, (D) 8, (E) 9, and (F) 10. The scale bars indicate 5 μm . 21
- 4.9 SEM images of Ag microstructures synthesized by reducing 0.667 M silver acetate with 31 mM hydrogen peroxide at different temperature of: (A) 5 $^{\circ}$ C, (B) 30 $^{\circ}$ C, (C) 40 $^{\circ}$ C, (D) 50 $^{\circ}$ C, (E) 60 $^{\circ}$ C, and (F) 80 $^{\circ}$ C. The scale bars indicate 1 μm . 22
- 4.10 Raman spectra and SEM images of Ag microstructures, silver acetate powder and Ag microplates. 23
- 4.11 SEM images and photographic images of Ag microstructures (A) before and (B) after a separation by ethyl acetate 24
- 4.12 SEM images of Ag microstructures synthesized from the chemical reaction with the present of saturated organic solvent in the reaction media: as-synthesized structures (A) ethyl acetate, (B) butyl acetate, (C) hexane, and (D) toluene, 24 h incubated

- structures (E) ethyl acetate, (F) butyl acetate, (G) hexane, and (H) toluene. The scale bars indicate 5 μm . 25
- 4.13 Ag microstructures synthesized while there was a splitting layer: (A) ethyl acetate, (B) butyl acetate, (C) hexane, and (D) toluene. 26
- 4.14 SEM images of Ag microstructures at the beginning period of time. The scale bars indicated 1 μm . 27
- 4.15 Fig.4.15 (A) Raman spectra of 10 mM R6G on different Ag microstructures, (B) bar graph plots between Raman intensity and Ag microstructures and SEM images (a-d) of different Ag microstructures. The scale bars of SEM images indicate 1 μm . 27
- 4.16 Schematic drawing of Raman detection showing the volume of excitation. 29
- 4.17 Raman spectra of R6G on Ag microstructures. 30
- 4.18 Raman spectra of (A) food wraps and (B) Ag microstructures that placed on the food wrap and transfer to glass slide. 31

LIST OF TABLES

Table	Page
1.1 Some previous research about synthesis of Ag dendrites	1



LIST OF ABBREVIATIONS

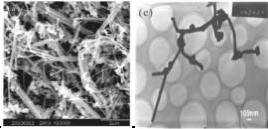
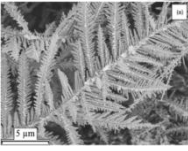
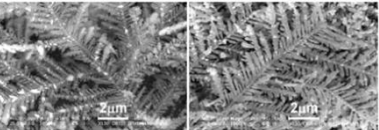
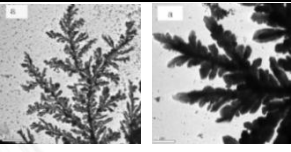
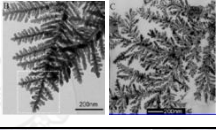
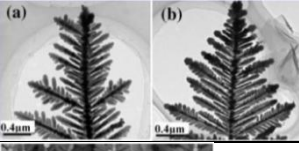
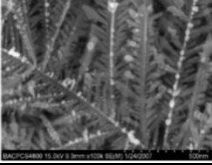
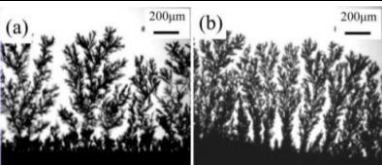
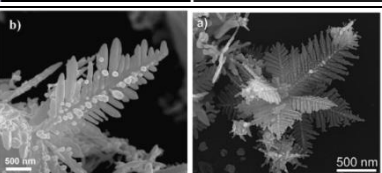
AgNO ₃	: silver nitrate
CH ₃ COONa	: sodium acetate
CH ₃ COOAg	: silver acetate
H ₂ O ₂	: hydrogen peroxide
CH ₃ COOCH ₂ CH ₃	: ethyl acetate
CH ₃ COOCH ₂ CH ₂ CH ₂ CH ₃	: butyl acetate
C ₇ H ₈	: toluene
C ₆ H ₁₄	: hexane
SERS	: Surface-enhanced Raman scattering
nm	: nanometer
μm	: micrometer
Ag	: silver (Argentum)
eV	: electron volt
SEM	: scanning electron microscopy
TEM	: transmission electron microscopy
EDS	: Energy-dispersive spectroscopy
XRD	: X-ray diffraction
TGA	: Thermogravimetric analysis
R6G	: Rhodamine 6G (C ₂₈ H ₃₁ N ₂ O ₃ Cl)

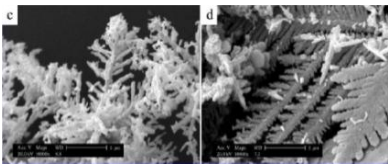
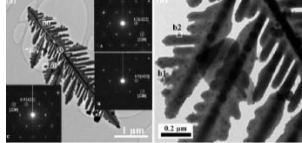
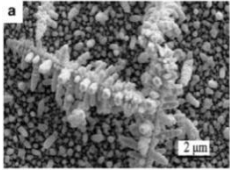

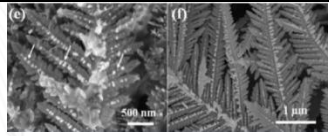
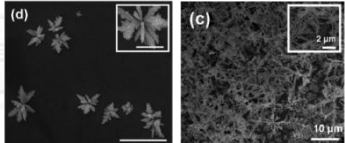
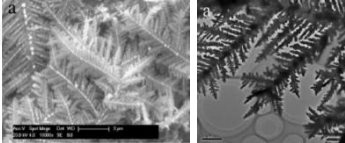
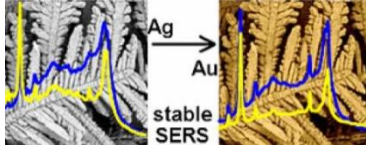
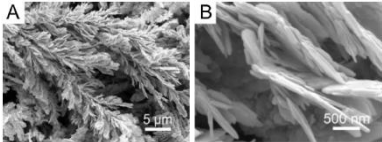
Chapter I

Introduction

The nanostructures of noble metals have been attractive in recent years due to their unique properties such as optical, electrical and thermal properties, as well as their potential applications in catalysis [1] and Surface-enhance Raman scattering (SERS) detection [2, 3]. The specific properties of the metal nanostructures can be tuned by controlling their shape and size. Many reports have shown the development of Ag nanostructures in different shapes, such as wires [4-6], belts [7], prisms [8], sheets [9], and other structures [10-14]. Recently, more complex structures such as hierarchical nanostructures have been synthesized with many methods because such materials have desirable applications. Since hierarchical structures are full with dendritic connections of nanowires, they provide high surface area and large amount of hot spots that are suitable for SERS technique. Most hierarchical structures reported so far based on synthetic methods such as electrochemical deposition [15, 16], surfactant process [17], γ - or ultrasonic irradiation [18], hydrothermal method [19], galvanic replacement [20], and chemical reaction [21, 22] as shown in Table 1. In general, the above methods involve the reduction of silver salts in the presence of organic surfactants and electron sources, and provide dendritic structures but such a SERS application unfortunately requires very clean Ag surface to allow probe molecules get electromagnetic field from Ag with no interference of capping agents. Therefore, it still remains interesting and challenging to synthesize Ag dendrite with more sophisticated but controllable through simpler routes, shorter time, and surfactant-free method under ambient conditions.

Table 1.1 Some previous research about synthesis of Ag dendrites.

Authors	Method	Reagent	Picture	Application
Guodan Wei, et al, Chem. Matter, 2003 [23]	Solvothermal method	AgNO ₃ +EG+PVP		
Kuiqing Peng and Jing Zhu, Electrochimica Acta, 2004 [24]	Galvanic replacement	AgNO ₃ +Si+HF		
Qin Zhou, et al., Materials letter, 2006 [15]	Electrodeposition	AgNO ₃ +Block copolymer123		
Lehui Lu, et al., J Phy Chem B, 2006 [22]	Chemical reaction	AgNO ₃ +p-aminobezine +NaBH ₄		Study of oriented attachment
Xiaogang Wen, et al., Langmier, 2006 [25]	Galvanic replacement	AgNO ₃ +Zn (powder)		SERS
Jixiang Fang, et al, Crystal Growth & Design, 2007 [26]	Galvanic replacement	AgNO ₃ +Zn (plate)		
Cuiyu Jing and Yan Fang, Colloid and Interface Science, 2007 [16]	Electrodeposition	AgNO ₃		SERS
Hongjun You. Et al., J Phy Chem C, 2008 [27]	Galvanic replacement	AgNO ₃ +Zn (plate)		Study of diffusion
Ved Varun Agrawal, et al., J colloid and interface science, 2008 [28]	Chemical reaction	AgNO ₃ +TOAB,CTAB+hydrazine		

Lei Fang and Rong Guo, Crystal Growth & Design, 2008 [17]	Chemical reaction	AgNO_3 +L-ascorbic acid+CTAB/SDBS		
Chandong Gu and Tong-Yi Zhang, Langmuir, 2008 [29]	Electrodeposition on Ni/Cu	AgNO_3		superhydrophobic for electrode
Weichun Ye, et al., Electrochemistry Communication, 2008 [30]	Galvanic replacement	AgNO_3 +Si+HF		SERS
Albert Gutés, et al., JACS Com., 2010 [31]	Galvanic replacement	$\text{AgF}+\text{Al}$		SERS
Gaixia Zhang, et al., Crystal Growth & Design, 2011 [21]	Galvanic replacement	AgNO_3 +Mg		
Digish K. Sharma, et al., Colloids and Surfaces, 2011 [32]	Electrodeposition	AgNO_3		SERS and reduction reaction
Xia Qin, et al., Langmuir, 2012 [33]	Electrodeposition on Au	AgNO_3		H_2O_2 reduction
Albert Gutés, et al., Langmuir, 2012 [34]	Galvanic replacement	$\text{AgF}+\text{Al}$		SERS
Wenya Cai, et al., Materials Research Bulletin, 2013 [35]	Galvanic replacement	$\text{CH}_3\text{COOAg}+\text{Cu}$		SERS

Nevertheless, most of the dendritic microstructures synthesis requires high concentration of surfactant to control Ag into dendritic structures, and also high

concentration of Ag to increase the yield, so AgNO₃ was chosen because of its high solubility. Moreover, synthesis of dendritic Ag by galvanic replacement needs more than 6 h and difficult to control the uniformity. Electrodeposition method is also too difficult to control structures, because they control the structures by adjusting the electrical potential and time, the dendritic structures occur on large surface of electrode. Therefore the structure cannot be uniform all over area of the electrode. Both techniques are not practical for SERS substrate preparation.

Based on the chemical reaction, we report a simple, rapid, green and no waste synthesis of the large scale synthesis of adjustable dendritic Ag microstructures. In this synthesis, H₂O₂ was used as a reducing agent to react with CH₃COOAg in aqueous solution and no organic solvent, surfactant or capping agents were necessary. This is the first time that dendritic Ag microstructures are made from H₂O₂ reduction. The precursor conditions and surface modification play a role as the morphological control of Ag structures. The morphological evolution of the dendritic Ag microstructures was also investigated through a series of time dependent SEM images, and the growth mechanism of Ag microstructures is also discussed.

Objective

Objective of the research is to synthesize controllable, rapid and practical dendritic Ag microstructures for SERS detection.

Benefit of the research

This research proposes another method to synthesize and control dendritic Ag microstructures which have desirable SERS property. This research also emphasizes the migration of harmful chemicals from food wrap using the advantage of dendritic Ag microstructures on SERS.

Chapter II

Theoretical background

In 1928, Raman and Krishnan first observed and reported inelastic light scattering from its feebleness in comparison to ordinary scattering [36]. Even in 1925, Smekal theoretically predicted this phenomenon [37], the inelastic light scattering is called “Raman scattering”. Whenever a photon ($h\nu$) hits a molecule, the molecule would absorb some energy to vibrate (bending, stretching, etc.) itself, the losing energy photon will be collected by a light detector, the change of the energy is vibrational energy of the molecule. Raman spectroscopy gives the same information to IR spectroscopy, but Raman spectroscopy technically uses Vis-NIR light and measures the wavelength change of the scattering light while IR spectroscopy measures the remaining intensity of absorbed IR light at each wavelength. On the other hand, Raman spectroscopy investigates the polarizability change of molecules, but IR spectroscopy does the polarity. The intensity of Raman scattering depends on magnitude of the change of polarizability, so aromatic molecules show more intense Raman scattering than aliphatic molecules.

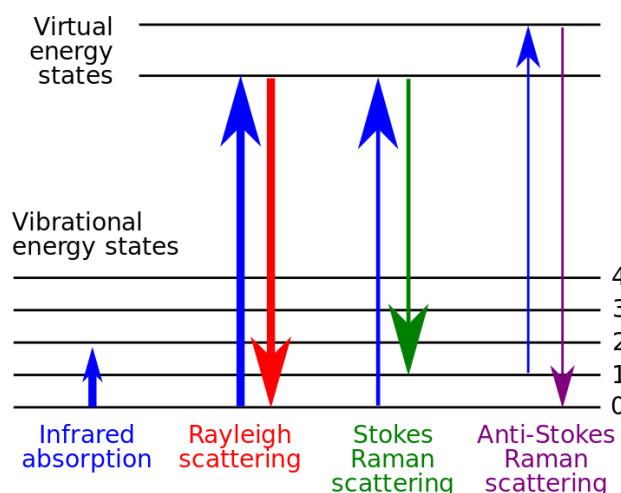


Fig.2.1 Energy-level diagram showing the states involved in Raman signal [38].

Raman scattering cross sections are much smaller than those of fluorescence, so Raman intensity is always weak. Raman spectroscopy uses single wavelength laser to excite the molecules, most of the scattering light do not change their energy (same wavelength as the laser which called Rayleigh scattering), but some of them lose or get the energy from the collision to the molecules are called Stokes or Anti-Stokes Raman scattering. Raman spectroscopy only focuses on Stokes Raman scattering, and the energy gaps of the change of wavelength confront to vibrational energy of the molecules. Accordingly, the possibility of Stokes scattering is very small, as well as only the light that scatters at the right angle can stimulate detector, Raman intensity is naturally low. Moreover, sensitivity limited of the detectors, and the intensity of the available laser have restricted the applications of Raman scattering for many years. However, the better light sources and light detectors are being developed to improve the disadvantages of the technique.

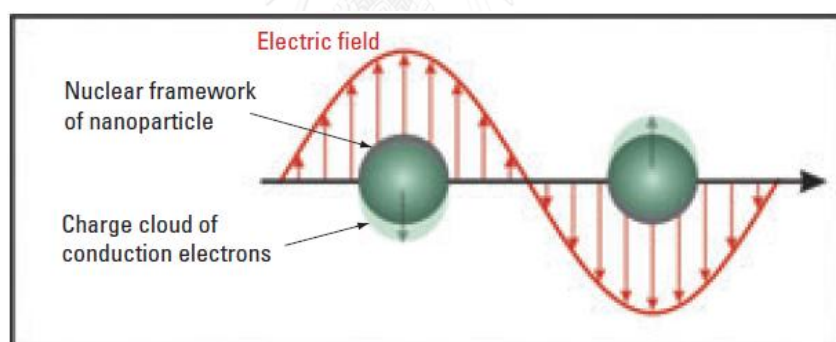


Fig.2.2 Illustration of the excitation of the LSPRs of a spherical nanoparticle by incident electromagnetic radiation. [39]

In 1977, Jeanmaire and Van Duyne conducted a research, which they placed the sample on or near a rough noble metal substrate, and they have found that the magnitude of Raman scattering signal is greatly enhanced [40]. They also conclude that strong electromagnetic fields can be generated when the localized surface plasmon resonance (LSPR) of nanoscale roughness features on a noble metal substrate is excited by visible light. When a molecule places on such a substrate,

electromagnetic fields from exciting laser and substrate both increase the possibility of inelastic scattering, and accordingly, the intensity increases. This phenomenon of enhancement is known as surface-enhanced Raman scattering (SERS), and most substrates are made of noble metals or their alloys.

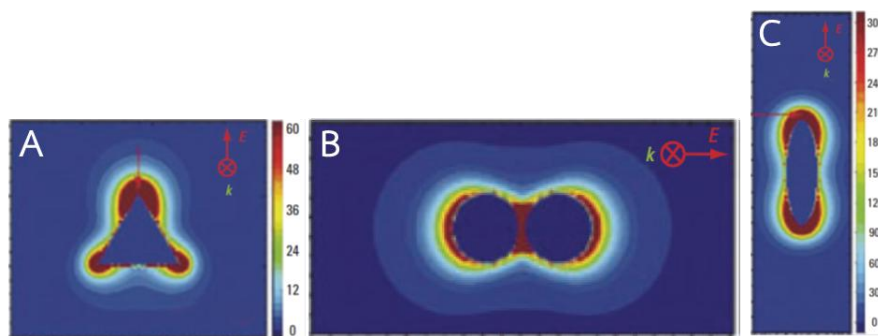


Fig.2.3 Theoretical simulations of the electromagnetic field enhancement around silver nanoparticles of (A) a triangular nanoparticle (700 nm), (B) a dimer of spherical nanoparticles (520 nm), and (C) an ellipsoidal nanoparticle (695 nm). [39]

According to SERS, Raman spectroscopy can be used for sensitive and specific molecular identification. Recently, SERS has been exploited to investigate in many applications such as analysis of pesticides [41], anthrax [42], specific antigen [43], glucose [44, 45], and nuclear waste [46]. It has also been implemented for identification of bacteria [47], genetic diagnostics [48], and immunoassay labeling [49-51]. Because of its practical sample preparation (no interference of water), portable device and low limit of detection, there have been many research in studying and making SERS substrate since SERS has been discovered. A number of SERS substrates can enhance the intensity even a single molecule can be also detected. To date, SERS technique is well known as a powerful analytical tool, and more than 200 papers about SERS are published every year.

The mechanism of SERS enhancement remains an active research topic. Since the discovery of the phenomenon, two major factors have disagreed on the relative significance of the proposed mechanisms: chemical enhancement and electromagnetic enhancement. In the chemical mechanism, which is now thought to

contribute an average enhancement factor of 100, a charge-transfer state is created between the metal and adsorbate molecules [52]. In a manner analogous to that observed in resonance Raman spectroscopy, the existence of this charge-transfer state increases the probability of a Raman transition by providing a pathway for resonant excitation. This mechanism is site-specific and analyte-dependent. The molecule must be directly adsorbed to the roughened surface to experience the enhancement.

To understand the electromagnetic enhancement, one must consider the size, shape, and material of the nanoscale roughness features. These characteristics determine the resonant frequency of the conduction electrons in a metallic nanostructure. When electromagnetic radiation with the same frequency is incident upon the nanostructure, the electric field of the radiation drives the conduction electrons into collective oscillation. Excitation of the LSPR has two consequences: selective absorption and scattering of the resonant electromagnetic radiation and generation of large electromagnetic fields at the surface of the roughness feature. Electromagnetic enhancement relies on Raman-active molecules being confined within these electromagnetic fields [53] and contributes an average enhancement factor of $\geq 10,000$.

Experiments

This chapter explains the synthesis and fabrication of Ag microstructures from silver acetate. The silver acetate salt was synthesized from the metathesis reaction between silver nitrate and sodium acetate in aqueous solution. The Ag microstructures were purified before implementing for Surface-enhance Raman substrate. The substrates were employed for the detection of plasticizers released from food wraps.

3.1 Chemicals and materials

- 3.1.1 Silver nitrate, AgNO_3 (Merck, analytical grade)
- 3.1.2 Sodium acetate tri-hydrate, $\text{CH}_3\text{COONa}\cdot 3\text{H}_2\text{O}$ (Merck, analytical grade)
- 3.1.3 Hydrogen peroxide, H_2O_2 (Merck, 30%w/w, analytical grade)
- 3.1.4 Sodium borohydride, NaBH_4 (Merck, 99.99%, analytical grade)
- 3.1.5 Ethyl acetate, $\text{CH}_3\text{COOCH}_2\text{CH}_3$, (Merck, analytical grade)
- 3.1.6 Butyl acetate, $\text{CH}_3\text{COO}(\text{CH}_2)_3\text{CH}_3$ (Merck, analytical grade)
- 3.1.7 Toluene, C_7H_9 (Merck, analytical grade)
- 3.1.8 Hexane, C_6H_{14} (Merck, analytical grade)
- 3.1.9 Rhodamine 6G, $\text{C}_{28}\text{H}_{31}\text{N}_2\text{O}_3\text{Cl}$, R6G (Merck, analytical grade)

3.2 Ag microstructures fabrication

This section explains the synthesis of Ag microstructures from the reaction between silver acetate and hydrogen peroxide. After the reaction, the Ag microstructures were purified for further usage as a SERS substrate.

3.3.1 Preparation of silver acetate

1. Prepare 1 M AgNO_3 solution (solution A) by dissolving 170 g AgNO_3 in 1 L of DI water.
2. Prepare 1 M CH_3COONa solution (solution B) by dissolving 138 g $\text{CH}_3\text{COONa}\cdot 3\text{H}_2\text{O}$ in 1 L of DI water.
3. Mix solution A and solution B under a vigorous stir. Solid silver acetate instantaneously precipitated as a white powder. The mixture was further stirred for 1 h in order to achieve a complete reaction.
4. Filter the white precipitate of silver acetate and wash 3 times with cold DI water.
5. Oven dry the filtrated silver acetate at 60°C for 12 h before keeping in a desiccator without exposure to a light source.

3.2.2 Preparation of saturated solution of silver acetate

1. Dissolve 12 g CH_3COOAg in 1 L DI water.
2. Heat the solution to 60°C for 1 h under a gentle stir to achieve a complete dissolution of CH_3COOAg .
3. Leave the solution undisturbed for 1 h to allow a precipitation of silver acetate crystal. The clear solution is the saturated silver acetate in DI water. The concentration of silver acetate was 0.667 M as determined by Mohr method. The saturated silver acetate solution was employed for further Ag microstructures fabrications.

3.2.3 Preparation of Ag microstructures

1. Inject hydrogen peroxide solution (15 μL , 9.76 M) into saturated solution of silver acetate (10 ml, 0.667 M) under a vigorous stir. The clear solution instantaneously turned turbid as silver ions were reduced into silver nanoparticles. Within 30 s, the colloid turned glittering as the nanoparticles developed into plate-shaped Ag microstructures. The

progress of the reaction was noticed by the formation of O_2 gas bubbles as hydrogen peroxide decomposed.

2. The colloid was further stirred for 2 min before leaving undisturbed for a precipitation of shiny Ag microstructures.
3. The Ag microstructures were separated from the solution by centrifugation before washing 3 times with DI water. They were kept in DI water for further usage.

3.2.4 The effects of experimental parameters on Ag microstructures

The effects of experimental parameters including concentration of Ag acetate, concentration of hydrogen peroxide, molar ratio Ag/CH_3COO^- , temperature and pH of hydrogen peroxide on the structures were conducted.

1. The effect of concentration of silver acetate: the procedures 1-3 in section 3.2.3 were conducted using the concentration of silver acetate 200, 267, 334, 400, 467, and 534 mM.
2. The effect of concentration of hydrogen peroxide: the procedures 1-3 in section 3.2.3 were conducted using the concentration of hydrogen peroxide 3, 15, 31, 154, 309, and 617 mM.
3. The effect of molar ratio of Ag/CH_3COO^- : procedure 1-3 in section 3.2.3 were conducted using 1:1, 1:2, 1:3, 1:4, 1:5, 1:6, 1:7, 1:8, 1:9 and 1:10.
4. The effect of pH of hydrogen peroxide: the procedures 1-3 in section 3.2.3 were conducted using hydrogen peroxide pH 1, 2, 3, 4, 5, 6, 7, 8, 9 and 10.
5. The effect of reaction temperature: the procedures 1-3 in section 3.2.3 were conducted using controlling temperature of the reactants 5, 28 (room temperature), 40, 50, 60 and $80^\circ C$.

3.3 Characterization

3.3.1 Optical microscopy

Few drops of suspended Ag microstructures were carefully dropped onto a (7.5x2.5 cm) glass slide. The glass slide was put on the slot of Zeiss optical microscope consisted of 5X, 10X, 50X, and 100X interchangeable objective lens and a pair of 10X eye piece.

3.3.2 Scanning Electron Microscopy (SEM)

The Ag microstructures that were already on the glass slide were contacted with a carbon tape-on-aluminium stub; the Ag microsheets were stuck on the carbon tape with adhesive material. The SEM sample was dried under vacuum machine for 30 minutes, then put in the SEM slot of Jeol JSM-6510A. Secondary electron scattering mode was used for characterization with 10kV voltage, and 1,000-50,000x magnification.

3.3.3 Raman scattering spectroscopy

A dispersive Raman from Thermo Scientific was operated to characterize the surface property. The dried Ag microstructures on the glass slide were beamed with a 532 nm laser in the condition of 0.5 mW, 0.5 second exposure time and 64 sample scans. The enhancement efficiency was tested by directly dropping various concentrations of R6G to the Ag microstructures and taken Raman spectrum.

3.3.4 Energy Dispersive spectroscopy (EDS)

The EDS samples were the same as those of SEM ones. The electron beam hit the sample with 20 kV to conduct the elemental analysis of the structures.

3.3.5 X-ray diffraction technique (XRD)

1 g of dried Ag microstructures were contained in an XRD sample slot then put in the XRD holder of 1X1X0.1 cm.



Chapter IV

Results and discussion

4.1 Fabrication of Ag microstructures

Ag microstructures were fabricated from the reaction between silver acetate (CH_3COOAg) and hydrogen peroxide (H_2O_2) at ambient temperature, and the results start demonstrating from the synthesis of silver acetate, Ag microstructures, structural controls, as well as the application as a SERS substrate.

4.1.1 Fabrication of silver acetate

Silver acetate (CH_3COOAg) occurs as a white-grayish powder constituted of needle-shaped crystals. The molecule of silver acetate is formed by the acetate ion covalently bonded to silver as an unidentate ligand; the unit cell in the crystalline solid is a $\text{Ag}_2(\text{carboxylate})_2$ dimer [54]. It is extensively used as a component in common pesticides, as industrial reagent and catalyst, in pharmaceutical industry and in the nanotechnology field. Silver acetate is also highly photo-sensitive, so the CH_3COOAg powder was kept in the dark.

White precipitate of silver acetate was prepared from a reaction between silver nitrate (AgNO_3) and sodium acetate (CH_3COONa); it appeared in the solution immediately after mixing of those reagents.

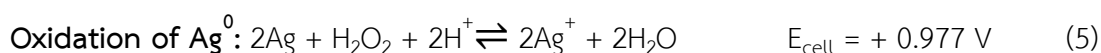
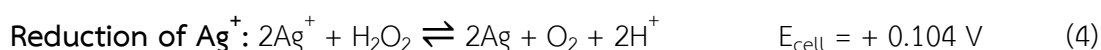
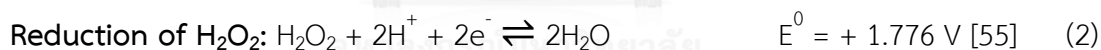


Fig.4.1 Optical and spectroscopic information of synthesized white silver acetate powder: (A) photographic image, (B) optical microscope image (100X magnification), and (C) SEM image.

White precipitate of silver acetate after drying in oven for 12 h is shown in Fig.1A, B, and C, and characterized by photography, optical microscopy, X-ray diffraction and scanning electron microscopy techniques. According to the SEM techniques, silver acetate shows crystal rod character with 200 μm in length and 10 μm in diameter. Fig.1D shows a Raman spectrum of silver acetate dominated by four peaks of C-O-Ag bending at 250 cm^{-1} , C-CH₃ in plane bending at 933 cm^{-1} , CH₃ bending at 1410 cm^{-1} , C-O-C stretching at 1340 cm^{-1} and CH₃ stretching at 2800 cm^{-1} [54].

4.1.2 Synthesis of Ag microstructures

Ag microstructures were fabricated by the reaction between silver acetate and hydrogen peroxide as follows:



A molecule of H₂O₂ supplies two electrons to silver ions both in acidic and alkaline conditions, and E_{cell} of the whole reaction is greater than zero which indicates that the reaction is spontaneous reaction.

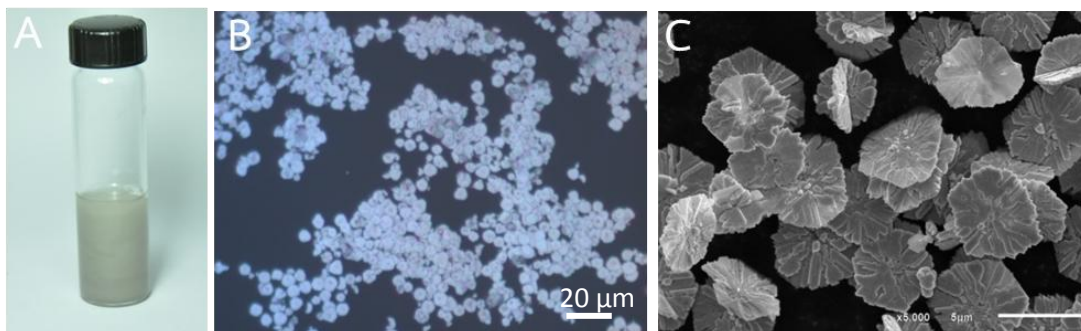


Fig.4.2 Ag microstructures prepared by a wet chemical reaction between silver acetate and hydrogen peroxide without surfactant or capping agent: (A) photographic image of the microstructures suspended in the reaction media, (B) optical microscope image (400X), and (C) SEM image.

The clear solution turned turbid as shown in Fig.4.2A within 15 s after H_2O_2 was injected, while glitters of Ag microstructures and O_2 bubbles appeared in the stirred solution. When the suspended O_2 bubbles were not noticeable, the stir was stopped (normally in 2 min of reaction time), and accordingly, Ag microstructures slowly settled. The Ag microstructures were separated for further experiments, and the solution containing leftover CH_3COOAg and H_2O_2 (H_2O_2 might not remain because of small amount usage and catalytic decomposition on Ag surface) was kept to reuse and recrystallized CH_3COOAg .

The Ag microstructures synthesized from 0.667 M CH_3COOAg and 31 mM H_2O_2 shown in Fig.4.2 have quite uniform plate shape with the lateral size of 4-6 μm and thickness of 150-200 nm. The edge and surface are rough. The pattern of roughness shows that the Ag microstructures are made of many nanopetals.

Because the reaction between CH_3COOAg and H_2O_2 is spontaneous and rapid, the reaction was incubated for 24 h to observe the change of Ag microstructures at 2 min and 24 h reaction time. As the results shown in Fig.4.3, Ag microstructures synthesized from 0.667 M CH_3COOAg and 31 mM H_2O_2 were taken at different reaction time, (A) 2 min and (B) 24 h, size and shape of Ag microstructures from Fig.4.3A are similar to one from Fig.4.2C indicating that the process is reproducible. Debris, triangular and polygonal of Ag microstructures was found in 24-

h incubated Ag microstructures shown in Fig.4.3B. As the results, the reaction media is active even H_2O_2 (the triggering reagent) might completely decomposed along 24 h under catalytic decomposition by Ag and neutral pH. During the long period of reaction time, active species could destroy Ag while selected forms of Ag were generated and survived.

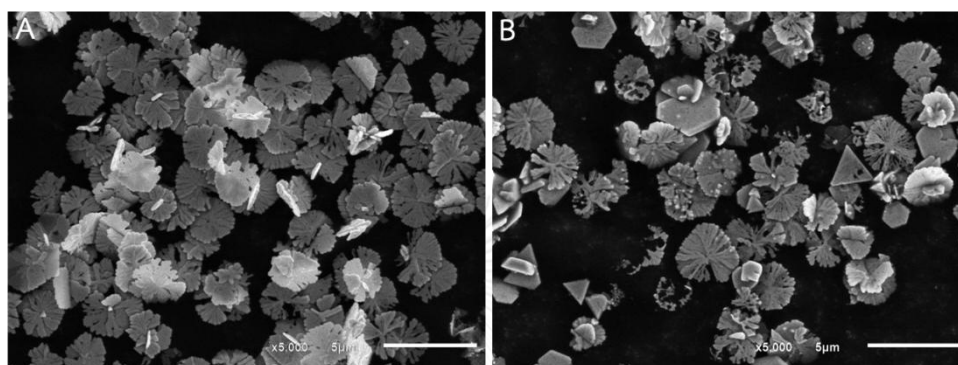


Fig.4.3 SEM images of Ag microstructures prepared by a wet chemical reaction between silver acetate and hydrogen peroxide without surfactant or capping agent: (A) as-synthesized and (B) 24 h incubation in the reaction media. The scale bars indicate 5 μm .

4.1.3 Characterization of Ag microstructures

Ag microstructures synthesized from CH_3COOAg and H_2O_2 were characterized. Elemental analysis was conducted with Energy dispersive spectroscopy, and X-ray diffraction. As the results shown in Fig.4.4, EDS Ag map (B) overlays on the Ag microstructures area in SEM image (A), EDS O map (C) does not give significant information, and EDS C map (D) indicates carbon tape under Ag microstructures which is the substrate. EDS spectrum in Fig.4.4F also confirms that Ag microstructures mainly consists of Ag, carbon peak is from carbon tape. Fig.4.4G is an X-ray diffraction (XRD) pattern of the same Ag microstructures used in EDS characterization. The four diffraction peaks can be indexed to diffraction from the (111), (200), (220) and (311) of faced-centered cubic (fcc) silver (JCPDS Card File, 4-783).

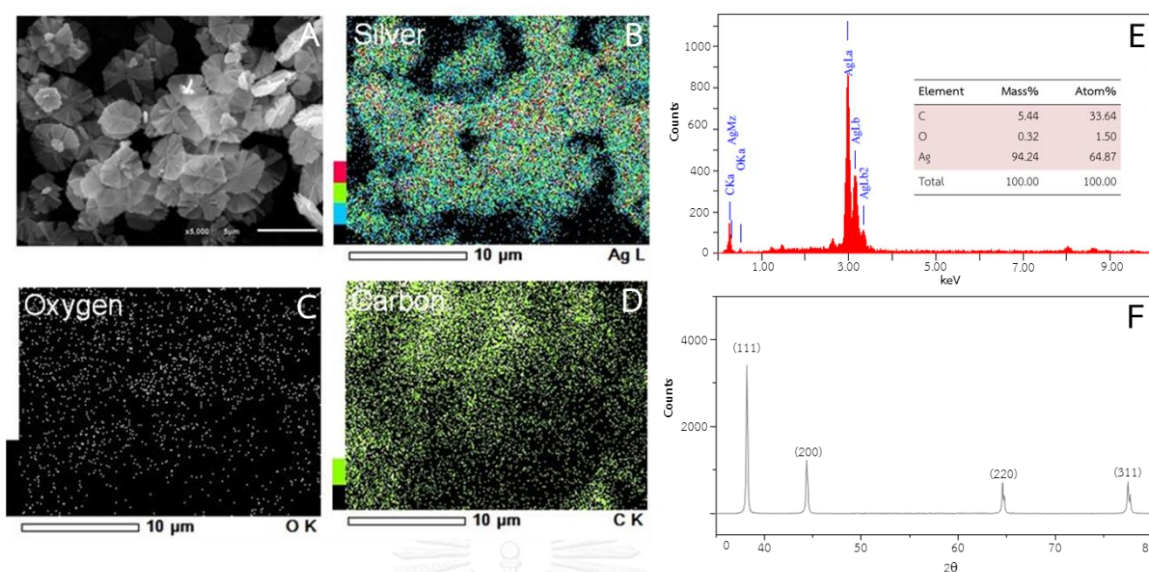


Fig.4.4 Elemental analysis of Ag microstructures: (A) SEM image, (B) EDS silver map, (C) EDS oxygen map, (D) EDS carbon map, (E) EDS spectrum, and (F) XRD pattern.

4.1.4 Effects of parameters to Ag microstructures

1. Effect of $[\text{CH}_3\text{COOAg}]$

Concentration of CH_3COOAg was varied to observe the effect of Ag source quantity to the Ag microstructures synthesized with fixed H_2O_2 concentration. The highest concentration of CH_3COOAg is 0.667 M (667 mM) which is saturated solution; other concentrations were diluted with DI water into 200, 267, 334, 400, 467, and 534 mM. The reaction at low concentrations of CH_3COOAg was not as fast as higher ones which showed the progress of the reaction such as glitter of Ag and O_2 bubbles rapidly instantly after mixing of the precursors. As the results shown in Fig.4.5, Ag microstructures obtained from 200 mM show polygonal microplates with diameter 3-5 μm , and have less population than others. Ag microstructures obtained from the reaction between 267 mM CH_3COOAg and 31 mM is shown in Fig.4.5B, the structures show more roughness at the edges and surface. Ag microstructures obtained from more concentrated CH_3COOAg show more complex structures.

Concentration of CH_3COOAg controls the population and the rate of reaction. The number of Ag^+ in CH_3COOAg directly specifies the population of Ag microstructure, and controls the probability of the collision between two reactants which affects rate of the reaction.

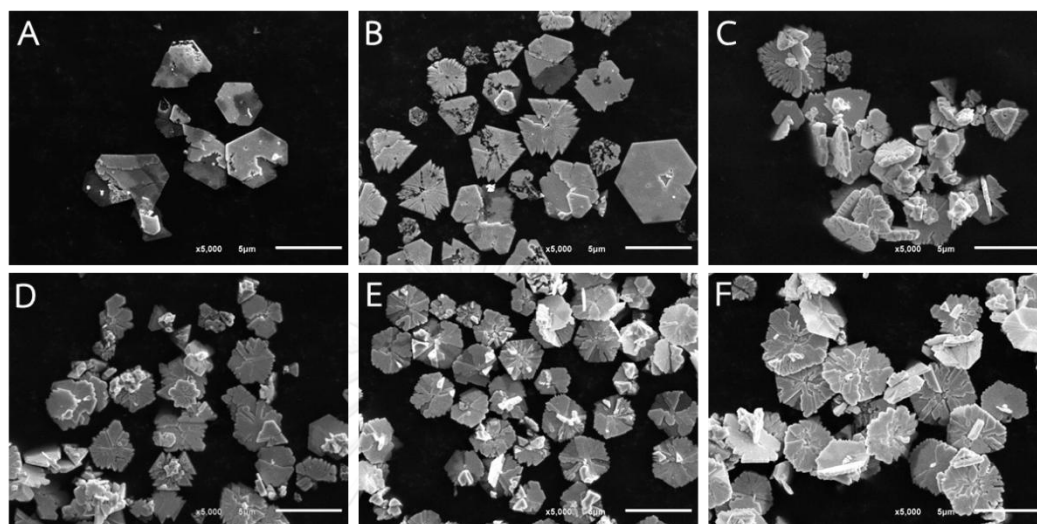


Fig.4.5 SEM images of Ag microstructures synthesized by reducing silver acetate with 31 mM hydrogen peroxide. The concentrations of silver acetate are: (A) 200 mM, (B) 267 mM, (C) 334 mM, (D) 400 mM, (E) 467 mM, and (F) 534 mM. The scale bars indicate 5 μm .

2. Effect of $[\text{H}_2\text{O}_2]$

Various concentrations of hydrogen peroxide (H_2O_2), 3, 15, 31, 154, 309, and 617 mM, were used to react with 0.667 M CH_3COOAg in order to observe the interference of H_2O_2 to the Ag microstructures. At low concentration of the electron donor, 3 mM H_2O_2 reacted with 0.667 M CH_3COOAg as shown in Fig.4.6A, the solution slowly turned turbid and generated particles. Ag microstructures have uniform plate shape with 3-4 μm of lateral size and 150-200 nm of thickness. The roughness and groove of Ag microstructures surface showed dendritic pattern, and the edges were also rough. When increase H_2O_2 concentration to 15 mM (Fig.4.6B), the reaction generated Ag glitter and O_2 bubbles faster than the previous batch. The obtained Ag microstructures were uniform in lateral size of 4-5 μm and thickness of 150-200 nm, and the roughness still showed dendritic pattern on the surface.

Moreover, some parts of microplates such as petals and incomplete plates were also found. The concentration of H_2O_2 reacted with 0.667 M CH_3COOAg was systematically increased to 31 mM (Fig.4.6C). The reaction rate was higher as the turning turbid of the solution making O_2 bubbles and Ag microstructures. Size of Ag microstructures was smaller to 2-3 μm , but the shape was still uniform even some incomplete structures were also found. The uniformity decreased when the concentration of H_2O_2 increased to 154 mM (Fig.4.6D); Ag microstructures in size of 0.5-4 μm together with triangular and polygonal structures were found. The rate of the reaction was also faster. The concentration of H_2O_2 was increased to 617 mM (Fig.4.6F). Accordingly, the reaction rate was increased, and the less uniformity showed. Ag^+ ions were converted to the shape of dendritic and triangular plates, quasi-spheres and other forms of Ag microstructures.

H_2O_2 was the only reducing agent in the system, and its concentration also controls the rate of reaction. The number of H_2O_2 molecules indicates the probability of the reaction, so the rate of reaction also depends on reducing agent concentration. The faster reaction generates smaller Ag microstructures because many unstable particles at the early reaction time aggregate as fast as they could to minimize the surface energy on the closest aggregated particles.

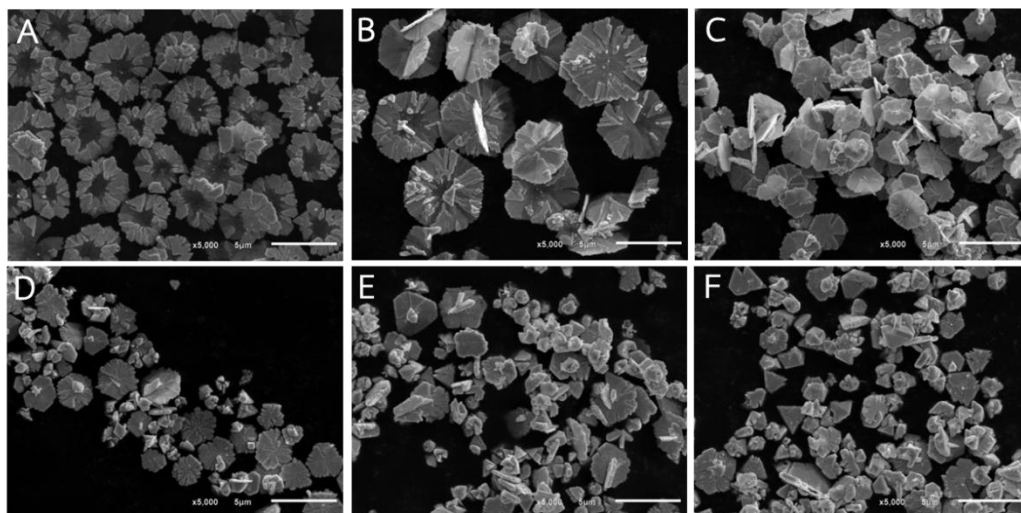


Fig.4.6 SEM images of Ag microstructures synthesized by reducing silver acetate with various concentrations of hydrogen peroxide: (A) 3 mM, (B) 15 mM, (C) 31 mM, (D) 154 mM, (E) 309 mM, and (F) 617 mM. The scale bars indicate 5 μm .

3. Effect of $[\text{CH}_3\text{COO}^-]$

CH_3COOAg consists of a mole of CH_3COO^- and a mole of Ag. So, it is obvious that CH_3COO^- , counter ion, should play an important role in structural formation. In this report, CH_3COONa was implemented to observe the interference of CH_3COO^- to the formation of Ag microstructures. The exact amounts of CH_3COONa were systematically added into 0.667 M CH_3COOAg , and reacted with 31 mM H_2O_2 for 2 min. The SEM images of Ag microstructures synthesized in the added CH_3COONa are shown in Fig.4.7. Fig.4.7B shows an SEM image of Ag microstructures synthesized from one time added more CH_3COO^- than normal CH_3COOAg , Ag microstructures show smaller petals and the thickness is decreased. When the amount of CH_3COO^- was increased, the size was decreased, but they showed the second and third layers on the primary dendritic plate. In conclusion, the increasing of CH_3COO^- amount, Ag microstructures tend to form many layers and end up to 3D structures assembled from dendritic microplates.

CH_3COO^- is a counter ion, self-stabilizer and structural studies of Ag^+ in CH_3COOAg . Delgado, (2007) [56] theoretical and experimental confirmed that carboxylate group strongly bound to Ag surface by catching its both O atoms onto Ag

surface and pointing CH_3 group perpendicular to the plane. The structural formation of Ag microstructures was changed when the amount of CH_3COO^- changed. According to the results, CH_3COO^- properly blocks Ag surface, and adatoms cannot thicken the Ag microstructures, so they grow another layer onto the first ones. The repulsion of CH_3COO^- on the surface also splits one sheet or petal out of another.

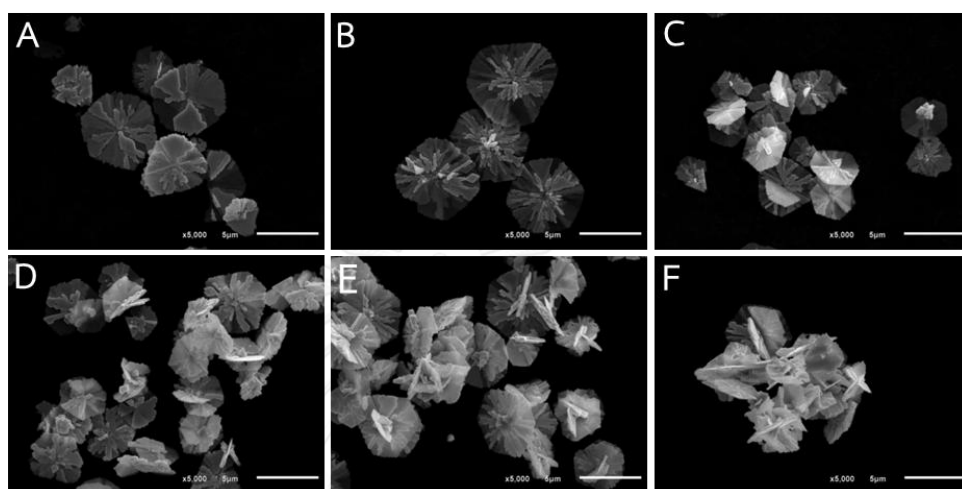


Fig.4.7 SEM images of Ag microstructures synthesized by reducing 0.667M silver acetate with 31 mM hydrogen peroxide. The concentrations of added sodium acetate are: (A) 0 M, (B) 0.667 M, (C) 2.668 M, (D) 4.002 M, (E) 5.336 M, and (F) 6.67 M. The scale bars indicate 5 μm .

CHULALONGKORN UNIVERSITY

4. Effect of pH of hydrogen peroxide

H_2O_2 is well known as a strong oxidizing agent, but it is implemented as a reducing agent for CH_3COOAg . H_2O_2 does not react with AgNO_3 (pH 4) because acidic condition is not suitable for reducing efficiency of H_2O_2 , but it does with CH_3COOAg and Ag_2O because they are neutral. CH_3COOAg (pH 7) is suitable for H_2O_2 reduction, and the higher pH also increases the reducing efficiency. The pH of CH_3COOAg solution could not be adjusted because increasing of the solution pH higher than 7 causes Ag_2O formation. However, the effect of pH to structural formation of Ag microstructures was conducted by adjusting pH of H_2O_2 . Various pH of 31 mM H_2O_2 (pH 5–10) were reacted with 0.667 M CH_3COOAg . As the results shown in Fig.4.8, the

higher pH of H_2O_2 affected Ag microstructures to less complex, smaller (from 3-5 μm to 0.5 μm) with the faster reaction rate.

The pH of the H_2O_2 can control growth of Ag microstructures by changing rate of the reaction which can be observed by size of Ag microstructures. The smaller structures and losing of dendritic pattern indicate the faster formation. Adjusting the pH of H_2O_2 results in change of size, shape and roughness on Ag microstructures.

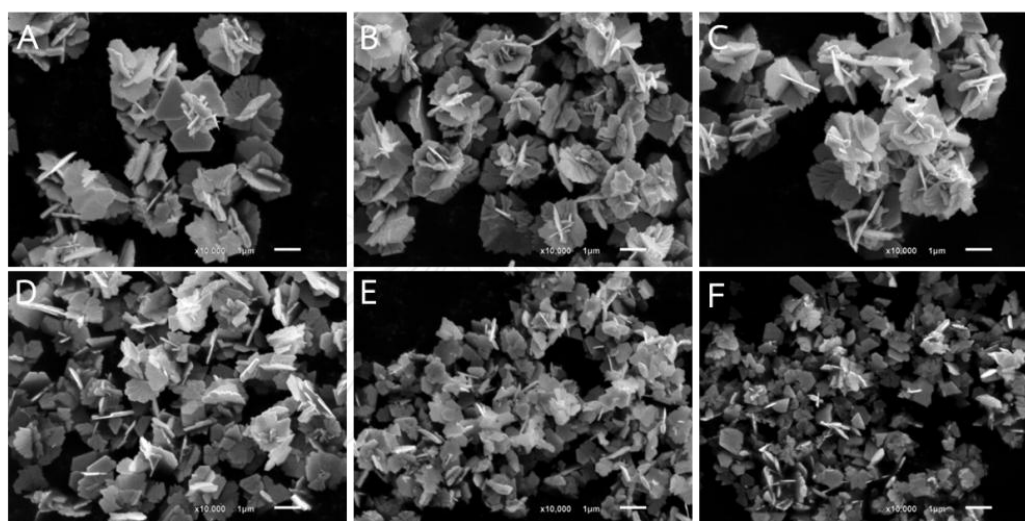


Fig.4.8 SEM images of Ag microstructures synthesized by reducing 0.667 M silver acetate with 31 mM hydrogen peroxide. The pH of hydrogen peroxide are: (A) 5, (B) 6, (C) 7, (D) 8, (E) 9, and (F) 10. The scale bars indicate 5 μm .

5. Effect of reaction temperature

The change of temperature can affect many reaction parameters such as activation energy, mobility, reaction rate, and other thermodynamic and kinetic parameters. So, the interference of temperature (5-80 $^{\circ}$ C) was investigated. As the results shown in Fig.4.9, the increase of temperature raised the reaction rate. At the higher temperature, the dendritic pattern was absence while other two forms of microstructures majored the population, which were quasi-sphere crystal and hexagonal plates.

The increasing temperature boosts the reaction rate by enhancing H_2O_2 decomposition, kinetic energy and activation energy accordingly, so Ag

microstructures form faster. In the highly active reaction, new generation particles have to reduce their surface energy by aggregating to one another. On the other hand, H_2O_2 also oxidizes the occurred particles, so the only selected Ag crystal structures survive in the solution. Most of seeds generated from H_2O_2 reduction are twin seeds, but multiple twin seeds can survive in H_2O_2 oxidation, the major populations at high reaction temperature are hexagonal plate and quasi sphere crystal which assembled from twin defects seeds [57, 58].

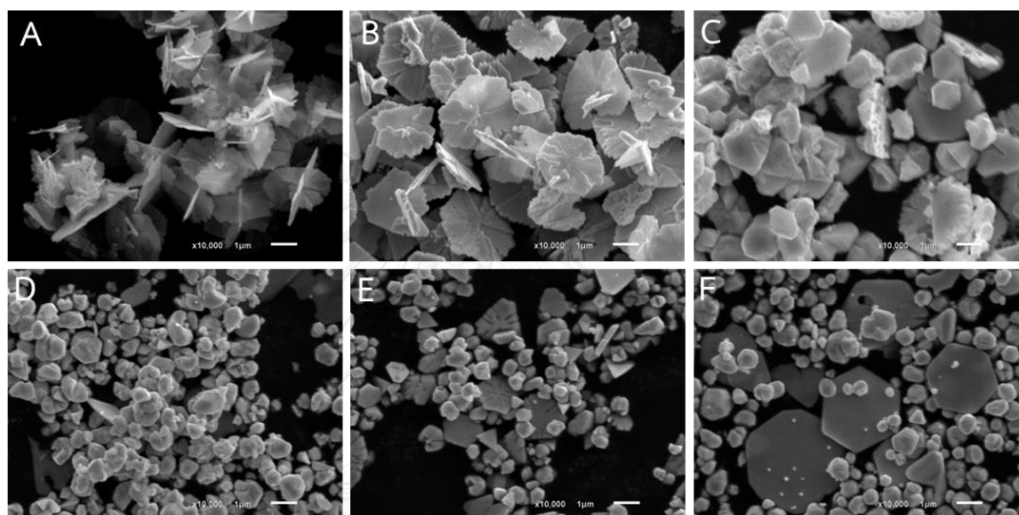


Fig.4.9 SEM images of Ag microstructures synthesized by reducing 0.667 M silver acetate with 31 mM hydrogen peroxide at different temperature of: (A) 5° C, (B) 30° C, (C) 40° C, (D) 50° C, (E) 60° C, and (F) 80° C. The scale bars indicate 1 μm .

4.2 Study of surface property

Ag microstructures synthesized from the reaction between 31 mM H_2O_2 and 0.667 M CH_3COOAg were characterized with Raman spectroscopy to investigate the surface property. According to the Raman spectra shown in Fig.4.10A, surface of Ag microstructures was covered with CH_3COOAg . After Ag microstructures being washed 3 times with DI water, the peak of C-H₃ in plane bending at Raman shift 933 cm^{-1} decreased, but the intensity of other peaks increase. On the other hand, Raman

spectrum of Ag microplates synthesized from $\text{Ag}(\text{NH}_3)_2^+$ [59] shows no vibrational signal. This indicates that surface of Ag microplates is clean.

Delgado, (2008) [60] demonstrated that Carboxylate groups strongly bind to Ag surface with their both O atoms and point the alkyl tail out perpendicular out of the surface. The CH_3COO^- also prefers to bind on (111) Ag and it is stable in the temperature lower than 300K [61]. According to the Raman spectra, Ag microstructures synthesized from CH_3COOAg and H_2O_2 spontaneously get CH_3COO^- on the surface.

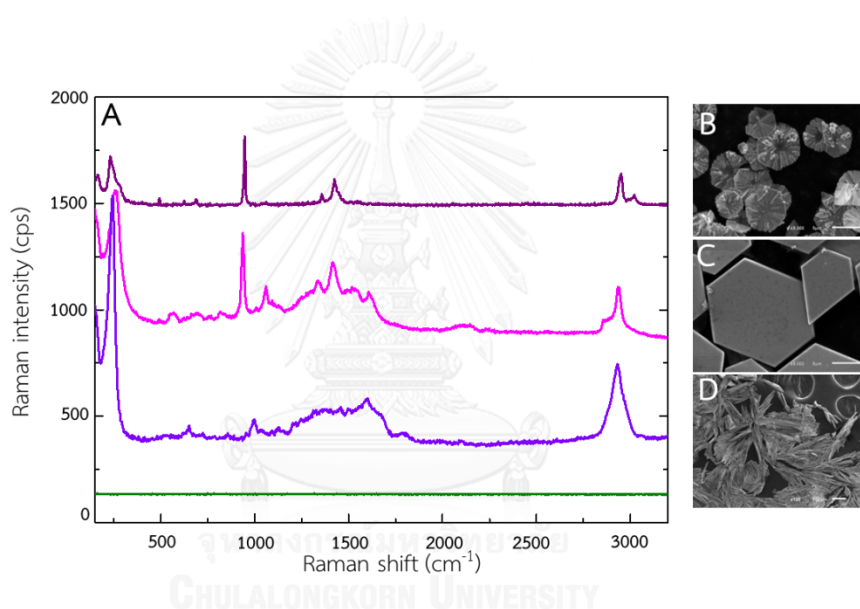


Fig.4.10 Raman spectra and SEM images of Ag microstructures, silver acetate powder and Ag microplates.

According to CH_3COO^- bound on Ag microstructures, ethyl acetate was added into the vial containing Ag microstructures which were synthesized with 31 mM H_2O_2 and 0.667 M CH_3COOAg , and shaken. The suspending Ag microstructures completely moved from water phase to the interface between ethyl acetate and water, and were left for 24 h. As the results shown in Fig.4.11, as-synthesized and 24-h Ag microstructures are identical. That indicates that organic layer can block Ag microstructures from the active species in aqueous solution.

Because of the alkyl tail of acetate group which points perpendicular to the Ag surface, ethyl acetate can easily bind with the hydrophobic group of the surface. The adding of ethyl acetate moves the Ag microstructures to the interface between aqueous/organic phases whenever it is shaken, since the separated layer of organic solvent cannot get to the Ag structures. Whenever the solution is shaken, the organic solvent splits as many droplets suspending in aqueous solution, and bind with Ag microstructures. The Ag microstructures that have been covered with organic molecules then cannot further be in aqueous solution, they move up with organic droplets to the organic/aqueous interface.

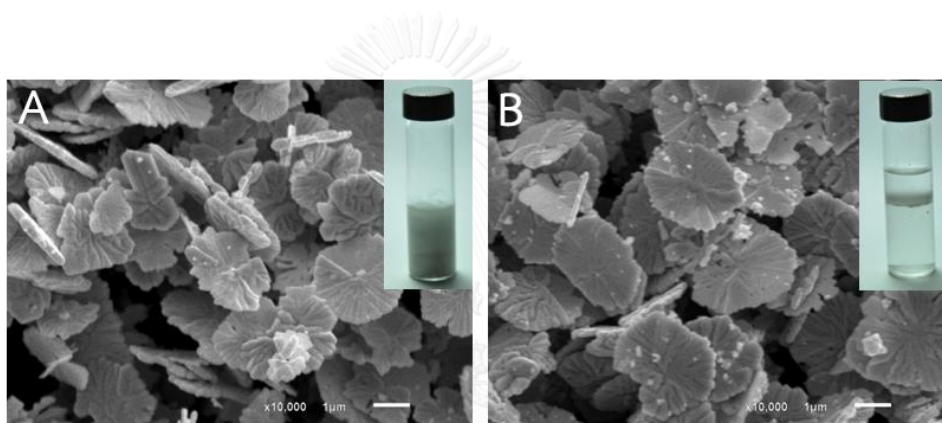
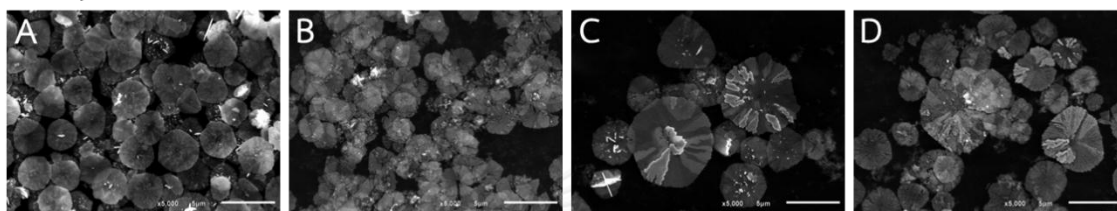


Fig.4.11 SEM images and photographic images of Ag microstructures (A) before and (B) after a separation by ethyl acetate. The scale bars indicate 1 μm .

Some organic solvents such as ethyl acetate, butyl acetate, toluene, and hexane were implemented to observe the effect of organic solvent to the formation of Ag microstructures. CH_3COOAg which contained each of those organic solvents was reacted with H_2O_2 and incubated for 24 h. SEM images of the Ag microstructures synthesized with the present of organic solvents show in Fig.4.12 (A-D) and (E-H); it is noticeable that they are different from each other and from Ag microstructures synthesized without organic solvent. The as-synthesized Ag microstructures obtained from the reaction which ethyl acetate saturated in CH_3COOAg were uniform in size of 2-3 μm and thickness of 10-15 nm (Fig.4.12A). Ag microstructures from butyl acetate were 1 μm wide and 5-10 nm thick (Fig.4.12B) while ones from hexane were various

size of 1-6 μm and 20-30 nm thick (Fig.4.12C). Ag microstructures obtained from the presence of toluene were also dendritic plate shape but varied-sized. The 24-h Ag incubated microstructures shown in Fig.4.12 (E-H) still reacted with active species in the solution. They were thicker and wider, but some of them lost their original structures because of the incomplete surface passivation of the organic solvents.

As-synthesized silver microstructures



24-h incubated silver microstructures

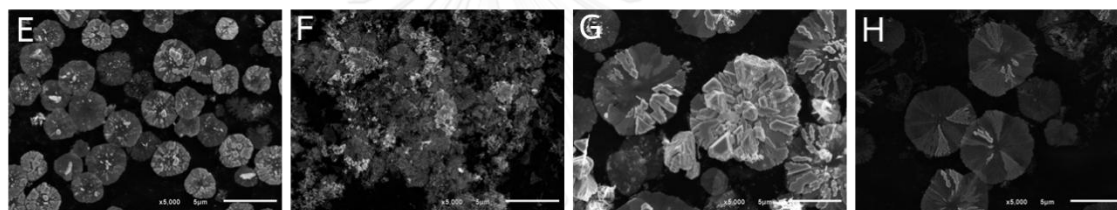


Fig.4.12 SEM images of Ag microstructures synthesized from the chemical reaction with the present of saturated organic solvent in the reaction media: as-synthesized structures (A) ethyl acetate, (B) butyl acetate, (C) hexane, and (D) toluene, 24 h incubated structures (E) ethyl acetate, (F) butyl acetate, (G) hexane, and (H) toluene. The scale bars indicate 5 μm .

Ag microstructures synthesized in the presence of organic solvent in the aqueous solution showed the interesting evidence on structural formation. So, organic solvents were used again to achieve the dendritic Ag structures. Such solvents were added into CH_3COOAg showing its layer on top of the solution, the reaction was then conducted with the mentioned process. Ag microstructures shown in Fig.4.13 indicate that they lose the uniformity, and most of them illustrated incomplete dendritic formation.

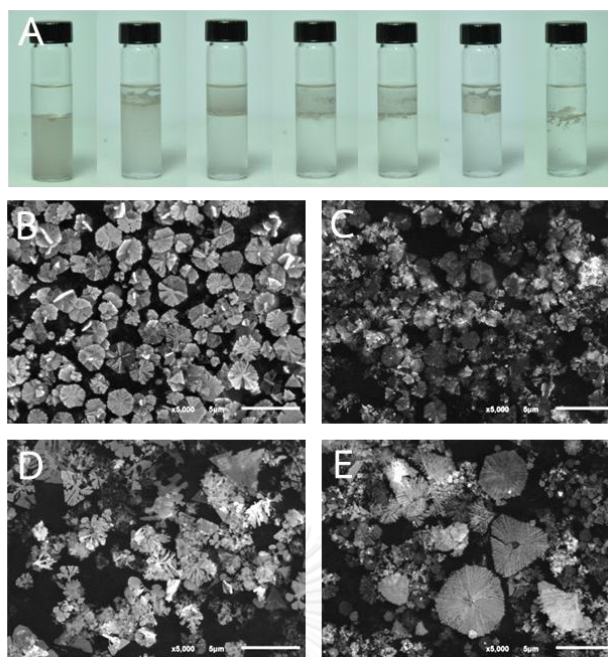


Fig.4.13 Ag microstructures synthesized while there was a splitting layer: (A) ethyl acetate, (B) butyl acetate, (C) hexane, and (D) toluene. The scale bars indicate 5 SEM images of Ag microstructures synthesized from the chemical reaction with the present of saturated organic solvent in the reaction media: as-synthesized structures (A) ethyl acetate, (B) butyl acetate, (C) hexane, and (D) toluene, 24 h incubated structures (E) ethyl acetate, (F) butyl acetate, (G) hexane, and (H) toluene. The scale bars indicate 5 μm .

4.3 Growth mechanism of Ag microstructures

Structural evolution of Ag microstructures was conducted with observing the Ag structures at first 5 s of reaction time (Fig.14). This indicates that Ag microstructures start symmetrically growing from a few primary branches, then secondary, tertiary and so on branches also grow from primary branches and finally form a dendritic disk shape. The angles between branches were $\sim 60^\circ$ which conformed to crystal orientation between (111) and (100) [22, 25, 26, 30, 31, 34]. The structural evolution indicates that Ag^+ ions were reduced by H_2O_2 generating Ag atoms, the Ag atoms tended to aggregate by a driving force of high surface energy. They clustered as Ag nanoparticles, and by the driving force of surface energy, they

repeatedly attached to one another with a preferred direction which called ‘oriented attachment’ [62]. Finally, Ag microstructures showed their high rough surface on plate shape and reflected as Ag mirror.

The faster reaction rate generates smaller particles [63, 64]. A number of Ag atoms nucleated at the first generation, and they instantly aggregated as Ag particles or Ag seeds to reduce the surface energy. The survival seeds continuously grew to form dendritic microstructures.

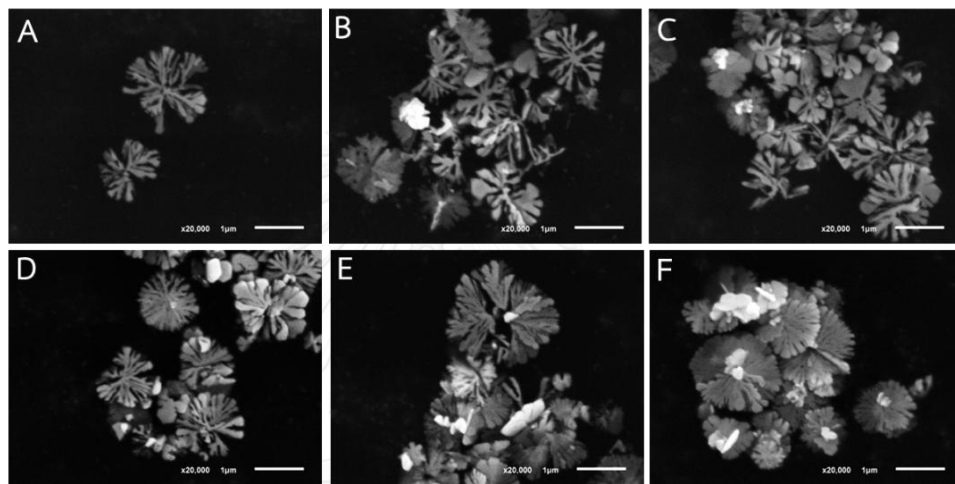


Fig.4.14 SEM images of Ag microstructures at the beginning period of time. The scale bars indicated 1 μm .

4.4 Application on Surface Enhance Raman Scattering substrate

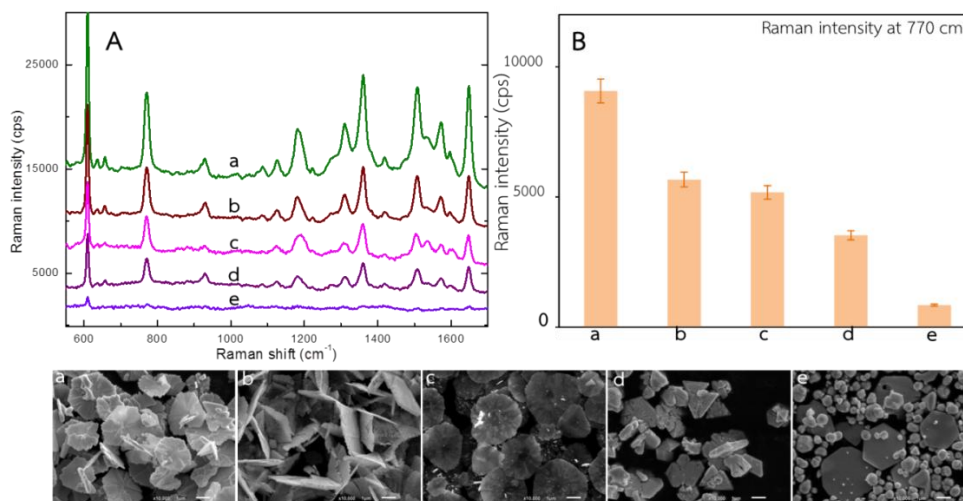


Fig.4.15 (A) Raman spectra of 10 μM R6G on different Ag microstructures, (B) bar graph plots between Raman intensity and Ag microstructures and SEM images (a-d) of different Ag microstructures. The scale bars of SEM images indicate 1 μm .

Five Ag microstructures synthesized from different conditions were implemented as Raman substrates, and R6G in the concentration of 10 μM was used as the probe molecules. As the result, dendritic Ag microstructures (Fig.4.15a) synthesized from 0.667 M CH_3COOAg and 31 mM H_2O_2 show the best enhancement efficiency noticeable by the bar graph in Fig.4.15B which compares the peak intensity at 770 cm^{-1} of five different Ag microstructures. The second best is 3D Ag microstructures synthesized with the same condition to Fig.4.15a, but the CH_3COONa was added to 1:8 of Ag/ CH_3COO^- molar ratio. The Ag microstructures synthesized with the above condition in the presence of ethyl acetate also are the third come in the Raman enhancing efficiency. The less dendritic pattern Ag microstructures shown in Fig.4.15d were also synthesized with the above condition, but the rate of reaction was increased by increasing concentration of H_2O_2 to 1%, and they still enhance the Raman signal. The Ag microstructures synthesized at 80 $^\circ\text{C}$ also enhance the Raman signal even in small efficiency.

As the result, the roughness on Ag microstructures represents Raman enhancing efficiency. The flat Ag microstructures (Fig.4.15a) have high roughness which assembled from a number of nanodendrites, which the molecules can place at the gap and get the electromagnetic field from the Ag structures. The 3D Ag microstructures assembled from dendritic Ag plate-like seeds can enhance Raman signal because of the dendritic pattern. But their enhancing efficiency cannot beat the first structures because the 3D structures scatter the light to every direction and block the excitation laser themselves. The Ag microstructures synthesized in the presence of ethyl acetate are thin, flat and highly dendritic structures, but their SERS efficiency does not as good as the first one because their surface was still hydrophobic that does not allow R6G molecules to penetrate into the nanogaps. The less rough, thicker and smaller Ag microstructures synthesized from increasing the concentration of H_2O_2 . They can enhance Raman signal, but not too high because of less surface area and nanogaps which indicate the number of molecules and generate the electromagnetic field, respectively. The Ag microstructures synthesized at $80^\circ C$ show $1\ \mu m$ quasi-sphere crystal structures and hexagonal plates. They also enhance the Raman signal, but not as good as others, because they no dendritic pattern which generates electromagnetic field. Even they do not have nanogaps; they can enhance the Raman signal with the junction between themselves.

According to the best enhancing structures, Ag microstructures synthesized with the chemical reaction between $0.667\ M\ CH_3COOAg$ and $31\ mM\ H_2O_2$ were implemented as a SERS substrate. An orange dye, Rhodamine 6G ($C_{28}H_{31}N_2O_3Cl$) was chosen as a probe molecule to observe Raman enhancing efficiency of the substrate. Various concentrations of R6G were dropped onto the substrate and taken Raman spectra. As the results shown in Fig.4.17, the Ag microstructures can detect R6G at concentration as low as $0.01\ nM$, while without the substrate; R6G at concentration of $1\ mM$ cannot be detected. The desirable SERS efficiency illustrates that Ag microstructures contain a number of hot spots which are the junctions of nanobranches. This is the potential of dendritic structure beyond other structures and the Ag microstructures could be a desirable Raman substrate. The detection

limit of the substrate has been determined by the numbers of molecules that were excited.

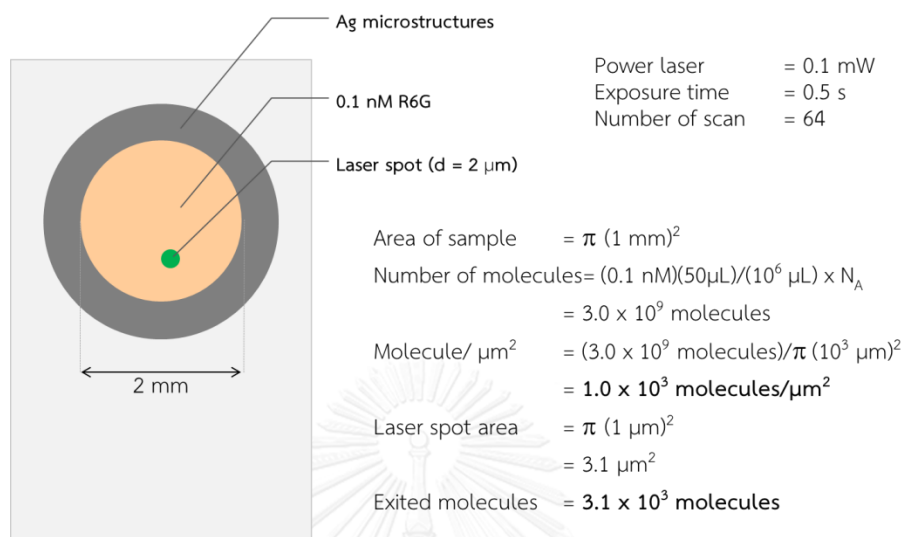


Fig.4.16 Schematic drawing of Raman detection showing the volume of excitation.

The volume that laser beam passes through the solution is the excited area which contained R6G in the portion of its concentration. Only those molecules scatter signal to Raman spectrometer, so the detection limit is about 3010 molecules of R6G. Even the Ag microstructures cannot enhance Raman signal to reach single molecule detection, the preparation of substrate is done simpler and faster. Moreover, the substrate does not require specific binding with probe molecule, thus it is widely available for many molecules.

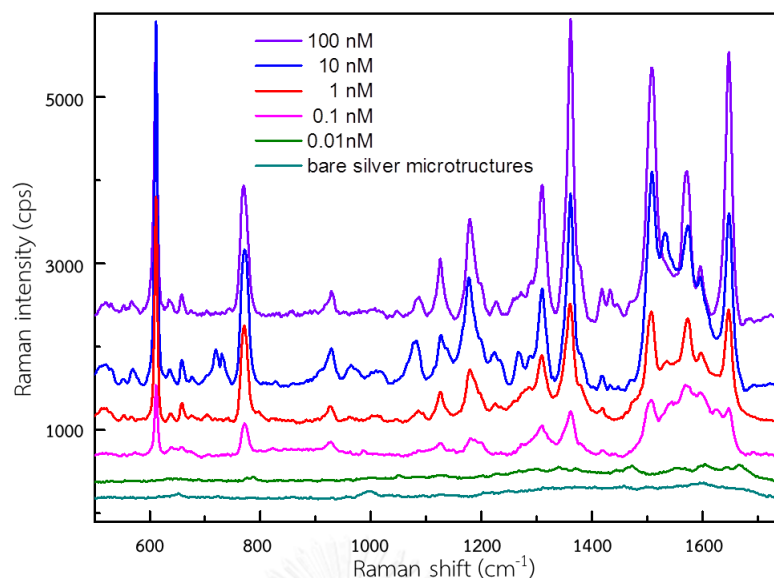


Fig.4.17 Raman spectra of R6G on Ag microstructures.

Nowadays, food wraps, mainly consist of poly (vinyl chloride), PVC, are widely used to cover leftover containers, food in stores and peeled fruits. They sometime directly contact to food and might release some chemicals. According to the potential of SERS property of the silver microstructures, they were tried as a Raman substrate to detect the chemicals released from food wraps.

Plastic wrap was first created from polyvinyl chloride (PVC), which remains the most common material. Non-PVC alternatives are now being sold due to concerns about the transfer of plasticizers from PVC into food, although PVC is still the most common. For some people, low density polyethylene (LDPE) is alternatively used instead of PVC-based ones. The PVC-based films contain plasticizers, most often bis(2-ethylhexyl) adipate (DEHA), but phthalates (most often dibutyl phthalate (DBP) and bis(2-ethylhexyl) phthalate (DEHP)) [65], in spite of being prohibited in most countries, also cause concern. The plasticizers were found to migrate to some foods, for example cheeses or fatty fish and meat.

Ag microstructures have been used as a sensor to detect plasticizers releasing from plastic wraps. The colloid of Ag microstructures was directly dropped onto 6 brands of plastic wraps bought from supermarkets and transferred them to clean

glass slide. According to the Raman spectra shown in Fig.4.18, they show a strong peak at 1000 cm^{-1} (C-OH stretching) which is not shown in wraps' spectra. We expect this peak is from plasticizers that migrate out of the wraps.

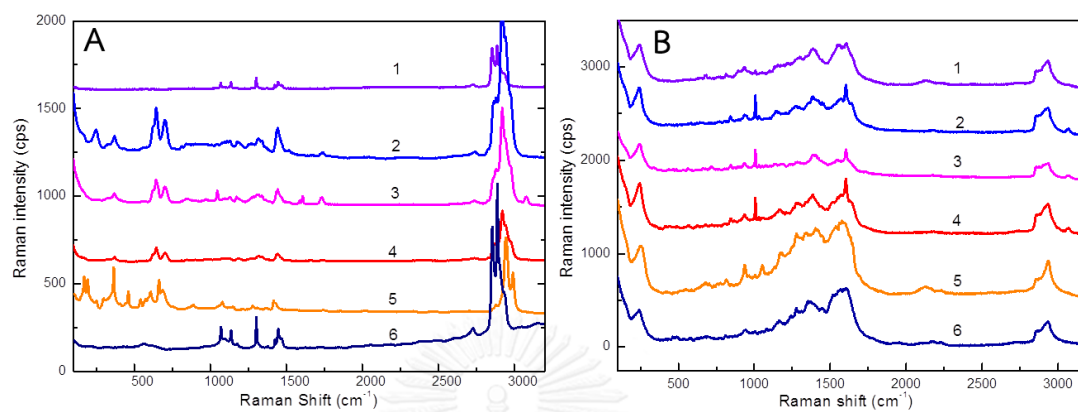


Fig.4.18 Raman spectra of (A) 6 brands of food wraps and (B) Ag microstructures that placed on the food wraps and transfer to glass slide.

Chapter V

Conclusions

In conclusion, the dendritic Ag microstructures (5-10 μm average diameter and 2-150 nm average thickness) have been synthesized by the reaction of hydrogen peroxide and silver acetate without stabilizer or capping agent operating in ambient condition. The kinetic change of the reaction controls the morphology of the structures, the increase of reaction rate made the thicker, smaller and less dendritic patterned Ag microstructures. Organic solvents also can move Ag microstructures from the aqueous media to organic/water interface by trapping to alkyl group at acetate ion attaching on the Ag surface. Moreover, dissolved organic solvent in reaction media also passivated then reduced the thickness of the Ag microstructures. In addition, the silver structures were placed as a Surface-enhanced Raman Scattering (SERS) substrate for R6G, probe molecule, exhibiting the detection limit as low as 0.1 nM because a plenty of nanogaps on the dendritic pattern generated a huge electromagnetic field then transferred to molecules in the gaps. Ag microstructures also have very well performance at detection of plasticizers in food wraps.

References

1. Kostowskyj, M.A., D.W. Kirk, and S.J. Thorpe, *Ag and Ag-Mn nanowire catalysts for alkaline fuel cells*. International Journal of Hydrogen Energy, 2010. **35**(11): p. 5666-5672.
2. Wiley, B.J., et al., *Synthesis and Optical Properties of Silver Nanobars and Nanorice*. Nano Letters, 2007. **7**(4): p. 1032-1036.
3. Nie, S. and S.R. Emory, *Probing Single Molecules and Single Nanoparticles by Surface-Enhanced Raman Scattering*. Science, 1997. **275**(5303): p. 1102-1106.
4. Sun, X.M. and Y.D. Li, *Cylindrical Silver Nanowires: Preparation, Structure, and Optical Properties*. Advanced Materials, 2005. **17**(21): p. 2626-2630.
5. Fang, J., et al., *Silver nanowires growth via branch fragmentation of electrochemically grown silver dendrites*. Chemical Communications, 2009(9): p. 1130-1132.
6. Lazzara, T.D., et al., *Polymer Templated Synthesis of AgCN and Ag Nanowires*. Chemistry of Materials, 2009. **21**(10): p. 2020-2026.
7. Liu, B., W. Luo, and X. Zhao, *A facile synthesis of ordered ultralong silver nanobelts*. Materials Research Bulletin, 2009. **44**(3): p. 682-687.
8. Xue, C., et al., *Mechanistic Study of Photomediated Triangular Silver Nanoprism Growth*. Journal of the American Chemical Society, 2008. **130**(26): p. 8337-8344.
9. Zhang, J.H., et al., *Controlling the Growth and Assembly of Silver Nanoprisms*. Advanced Functional Materials, 2007. **17**(9): p. 1558-1566.
10. Liu, X., et al., *Capping Modes in PVP-Directed Silver Nanocrystal Growth: Multi-Twinned Nanorods versus Single-Crystalline Nano-Hexapods*. Crystal Growth & Design, 2008. **8**(6): p. 1916-1923.
11. Nadagouda, M.N. and R.S. Varma, *Green synthesis of Ag and Pd nanospheres, nanowires, and nanorods using vitamin B₂: catalytic polymerisation of aniline and pyrrole*. J. Nanomaterials, 2008. **2008**: p. 1-8.

12. Tsuji, M., et al., *Roles of Pt seeds and chloride anions in the preparation of silver nanorods and nanowires by microwave-polyol method*. Colloids and Surfaces A: Physicochemical and Engineering Aspects, 2008. **316**(1–3): p. 266-277.
13. Zhang, W.C., et al., *Self-organized formation of silver nanowires, nanocubes and bipyramids via a solvothermal method*. Acta Materialia, 2008. **56**(11): p. 2508-2513.
14. Jena, B.K., B.K. Mishra, and S. Bohidar, *Synthesis of Branched Ag Nanoflowers Based on a Bioinspired Technique: Their Surface Enhanced Raman Scattering and Antibacterial Activity*. The Journal of Physical Chemistry C, 2009. **113**(33): p. 14753-14758.
15. Zhou, Q., et al., *Synthesis of highly crystalline silver dendrites microscale nanostructures by electrodeposition*. Materials Letters, 2006. **60**(29–30): p. 3789-3792.
16. Jing, C. and Y. Fang, *Simple method for electrochemical preparation of silver dendrites used as active and stable SERS substrate*. Journal of Colloid and Interface Science, 2007. **314**(1): p. 46-51.
17. Fan, L. and R. Guo, *Growth of Dendritic Silver Crystals in CTAB/SDBS Mixed-Surfactant Solutions*. Crystal Growth & Design, 2008. **8**(7): p. 2150-2156.
18. Wang, S. and H. Xin, *Fractal and Dendritic Growth of Metallic Ag Aggregated from Different Kinds of γ -Irradiated Solutions*. The Journal of Physical Chemistry B, 2000. **104**(24): p. 5681-5685.
19. Wang, Z., Z. Zhao, and J. Qiu, *A general strategy for synthesis of silver dendrites by galvanic displacement under hydrothermal conditions*. Journal of Physics and Chemistry of Solids, 2008. **69**(5–6): p. 1296-1300.
20. Xiao, J.P., et al., *Novel Ultrasonically Assisted Templated Synthesis of Palladium and Silver Dendritic Nanostructures*. Advanced Materials, 2001. **13**(24): p. 1887-1891.
21. Zhang, G., et al., *Morphology-Controlled Green Synthesis of Single Crystalline Silver Dendrites, Dendritic Flowers, and Rods, and Their Growth Mechanism*. Crystal Growth & Design, 2011. **11**(6): p. 2493-2499.

22. Lu, L., et al., *Oriented Attachment-Based Assembly of Dendritic Silver Nanostructures at Room Temperature*. The Journal of Physical Chemistry B, 2006. **110**(46): p. 23234-23241.
23. Wei, G., et al., *Self-organized Synthesis of Silver Chainlike and Dendritic Nanostructures via a Solvothermal Method*. Chemistry of Materials, 2003. **15**(23): p. 4436-4441.
24. Peng, K. and J. Zhu, *Morphological selection of electroless metal deposits on silicon in aqueous fluoride solution*. Electrochimica Acta, 2004. **49**(16): p. 2563-2568.
25. Wen, X., et al., *Dendritic Nanostructures of Silver: Facile Synthesis, Structural Characterizations, and Sensing Applications*. Langmuir, 2006. **22**(10): p. 4836-4842.
26. Fang, J., et al., *Dendritic Silver Nanostructure Growth and Evolution in Replacement Reaction*. Crystal Growth & Design, 2007. **7**(5): p. 864-867.
27. You, H., et al., *Morphological Evolution of Fractal Dendritic Silver Induced by Ions Walking within the Diffusion Layer*. The Journal of Physical Chemistry C, 2008. **112**(42): p. 16301-16305.
28. Agrawal, V.V., G.U. Kulkarni, and C.N.R. Rao, *Surfactant-promoted formation of fractal and dendritic nanostructures of gold and silver at the organic-aqueous interface*. Journal of Colloid and Interface Science, 2008. **318**(2): p. 501-506.
29. Gu, C. and T.-Y. Zhang, *Electrochemical Synthesis of Silver Polyhedrons and Dendritic Films with Superhydrophobic Surfaces*. Langmuir, 2008. **24**(20): p. 12010-12016.
30. Ye, W., et al., *Self-assembled synthesis of SERS-active silver dendrites and photoluminescence properties of a thin porous silicon layer*. Electrochemistry Communications, 2008. **10**(4): p. 625-629.
31. Gutés, A., C. Carraro, and R. Maboudian, *Silver Dendrites from Galvanic Displacement on Commercial Aluminum Foil As an Effective SERS Substrate*. Journal of the American Chemical Society, 2010. **132**(5): p. 1476-1477.

32. Sharma, D.K., et al., *The facile formation of silver dendritic structures in the absence of surfactants and their electrochemical and SERS properties*. Colloids and Surfaces A: Physicochemical and Engineering Aspects, 2011. **386**(1-3): p. 98-106.
33. Qin, X., et al., *Preparation of Dendritic Nanostructures of Silver and Their Characterization for Electroreduction*. Langmuir, 2012. **28**(11): p. 5218-5226.
34. Gutés, A., R. Maboudian, and C. Carraro, *Gold-Coated Silver Dendrites as SERS Substrates with an Improved Lifetime*. Langmuir, 2012. **28**(51): p. 17846-17850.
35. Cai, W., et al., *Facile fabrication of leafy spikes-like silver dendrite crystals for SERS substrate*. Materials Research Bulletin, 2013. **48**(10): p. 4125-4133.
36. Raman, C.V. and K.S. Krishnan, *A new type of secondary radiation*. Nature, 1928. **121**(3048): p. 501-502.
37. Smekal, A., *Zur quantentheorie der dispersion*. Naturwissenschaften, 1923. **11**(43): p. 873-875.
38. Lin-Vien, D., et al., *The handbook of infrared and Raman characteristic frequencies of organic molecules*. 1991: Elsevier.
39. Haynes, C.L., A.D. McFarland, and R.P.V. Duyne, *Surface-enhanced Raman spectroscopy*. Analytical Chemistry, 2005. **77**(17): p. 338 A-346 A.
40. Jeanmaire, D.L. and R.P. Van Duyne, *Surface raman spectroelectrochemistry: Part I. Heterocyclic, aromatic, and aliphatic amines adsorbed on the anodized silver electrode*. Journal of Electroanalytical Chemistry and Interfacial Electrochemistry, 1977. **84**(1): p. 1-20.
41. Liu, B., et al., *Shell Thickness-Dependent Raman Enhancement for Rapid Identification and Detection of Pesticide Residues at Fruit Peels*. Analytical Chemistry, 2011. **84**(1): p. 255-261.
42. Zhang, X., et al., *Rapid Detection of an Anthrax Biomarker by Surface-Enhanced Raman Spectroscopy*. Journal of the American Chemical Society, 2005. **127**(12): p. 4484-4489.

43. Grubisha, D.S., et al., *Femtomolar Detection of Prostate-Specific Antigen: An Immunoassay Based on Surface-Enhanced Raman Scattering and Immunogold Labels*. Analytical Chemistry, 2003. **75**(21): p. 5936-5943.
44. Shafer-Peltier, K.E., et al., *Toward a Glucose Biosensor Based on Surface-Enhanced Raman Scattering*. Journal of the American Chemical Society, 2002. **125**(2): p. 588-593.
45. Yonzon, C.R., et al., *A Glucose Biosensor Based on Surface-Enhanced Raman Scattering: Improved Partition Layer, Temporal Stability, Reversibility, and Resistance to Serum Protein Interference*. Analytical Chemistry, 2003. **76**(1): p. 78-85.
46. Bao, L., et al., *Silver-Doped Sol-Gel Film as a Surface-Enhanced Raman Scattering Substrate for Detection of Uranyl and Neptunyl Ions*. Analytical Chemistry, 2003. **75**(23): p. 6614-6620.
47. Jarvis, R.M., A. Brooker, and R. Goodacre, *Surface-Enhanced Raman Spectroscopy for Bacterial Discrimination Utilizing a Scanning Electron Microscope with a Raman Spectroscopy Interface*. Analytical Chemistry, 2004. **76**(17): p. 5198-5202.
48. Culha, M., et al., *Surface-Enhanced Raman Scattering Substrate Based on a Self-Assembled Monolayer for Use in Gene Diagnostics*. Analytical Chemistry, 2003. **75**(22): p. 6196-6201.
49. Cao, Y.C., R. Jin, and C.A. Mirkin, *Nanoparticles with Raman Spectroscopic Fingerprints for DNA and RNA Detection*. Science, 2002. **297**(5586): p. 1536-1540.
50. Doering, W.E. and S. Nie, *Spectroscopic Tags Using Dye-Embedded Nanoparticles and Surface-Enhanced Raman Scattering*. Analytical Chemistry, 2003. **75**(22): p. 6171-6176.
51. Mulvaney, S.P., et al., *Glass-Coated, Analyte-Tagged Nanoparticles: A New Tagging System Based on Detection with Surface-Enhanced Raman Scattering*. Langmuir, 2003. **19**(11): p. 4784-4790.

52. Campion, A. and P. Kambhampati, *Surface-enhanced Raman scattering*. Chemical Society Reviews, 1998. **27**(4): p. 241-250.
53. Schatz, G. and R. Van Duyne, *In Handbook of Vibrational Spectroscopy; Chalmers, JM; Griffiths, PR, Eds.* 2002, Wiley: New York.
54. Olson, L.P., et al., *The simple yet elusive crystal structure of silver acetate and the role of the Ag-Ag bond in the formation of silver nanoparticles during the thermally induced reduction of silver carboxylates*. Chemistry of Materials, 2006. **18**(6): p. 1667-1674.
55. Weast, R.C., M.J. Astle, and W.H. Beyer, *CRC handbook of chemistry and physics*. Vol. 69. 1988: CRC press Boca Raton, FL.
56. Delgado, J.M., A. Rodes, and J.M. Orts, *B3LYP and in Situ ATR-SEIRAS Study of the Infrared Behavior and Bonding Mode of Adsorbed Acetate Anions on Silver Thin-Film Electrodes*. The Journal of Physical Chemistry C, 2007. **111**(39): p. 14476-14483.
57. Guerrero-Martinez, A., et al., *Nanostars shine bright for you Colloidal synthesis, properties and applications of branched metallic nanoparticles*. Current Opinion in Colloid & Interface Science, 2011. **16**(2): p. 118-127.
58. Rodriguez-Lorenzo, L., et al., *Intracellular mapping with SERS-encoded gold nanostars*. Integrative Biology, 2011. **3**(9): p. 922-926.
59. Gatemala, H., C. Thammacharoen, and S. Ekgasit, *3D AgCl Microstructures Selectively Fabricated via a Cl--Induced Precipitation from [Ag (NH₃)₂]⁺*. CrystEngComm, 2014.
60. Berger, T., et al., *Formate Adsorption onto Thin Films of Rutile TiO₂ Nanorods and Nanowires*. Langmuir, 2008. **24**(24): p. 14035-14041.
61. Parker, B., B. Immaraporn, and A.J. Gellman, *Carboxylic Acid Deprotonation on the Ag(110) and Ag(111) Surfaces*. Langmuir, 2001. **17**(21): p. 6638-6646.
62. Penn, R.L. and J.F. Banfield, *Imperfect oriented attachment: dislocation generation in defect-free nanocrystals*. Science, 1998. **281**(5379): p. 969-971.
63. Richards, V.N., N.P. Rath, and W.E. Buhro, *Pathway from a Molecular Precursor to Silver Nanoparticles: The Prominent Role of Aggregative Growth*. Chemistry of Materials, 2010. **22**(11): p. 3556-3567.

64. Wang, F., et al., *Kinetics and Mechanisms of Aggregative Nanocrystal Growth*. Chemistry of Materials, 2013. **26**(1): p. 5-21.
65. Goulas, A.E., et al., *Migration of di(2-ethylhexyl) adipate and acetyltributyl citrate plasticizers from food-grade PVC film into sweetened sesame paste (halawa tehineh): Kinetic and penetration study*. Food and Chemical Toxicology, 2007. **45**(4): p. 585-591.



REFERENCES



APPENDIX



VITA

Name: Mr. Parinton Jangtawee

Date of Birth: June 16, 1989 Birth place: Yala, Thailand

Address: 59/55 Sateng Nok district, Amphore Muang, Yala, Thailand,

E-mail address: parinton_sp3@yahoo.com

Education:

2007 Bachelor of Science in Chemistry

Prince of Songkla University, Hatyai, Thailand

2009 Master of Science in Chemistry

Chulalongkorn University, Thailand

Conferences:

January 23-25, 2013 The 30th Annual Conference of the microscopy of Thailand, Thailand

January 8-10, 2014 Pure and Applied Chemistry International Conference 2014, Thailand

January 29-31, 2014 The 31st Annual Conference of the microscopy of Thailand, Thailand

August 10-15, 2014 International Conference on Raman spectroscopy, Germany

Awards:

January 8-10, 2014 Outstanding oral presentation on Physical Chemistry section in Pure and Applied Chemistry International Conference 2014, Thailand

